Monthly Notices of the ROYAL ASTRONOMICAL SOCIETY

MNRAS **546,** 1–17 (2026) https://doi.org/10.1093/mnras/stag108
Advance Access publication 2026 January 19

The galaxy–environment connection revealed by constrained simulations

Catherine Gallagher,[1]★ Tariq Yasin [1], Richard Stiskalek,[1,2] Harry Desmond [3] and Matt J. Jarvis [1]

[1]*Astrophysics, University of Oxford, Denys Wilkinson Building, Keble Road, Oxford OX1 3RH, UK*
[2]*Center for Computational Astrophysics, Flatiron Institute, 162 5th Ave, New York, NY 10010, USA*
[3]*Institute of Cosmology & Gravitation, University of Portsmouth, Dennis Sciama Building, Portsmouth PO1 3FX, UK*

Accepted 2025 December 23. Received 2025 December 23; in original form 2025 March 18

ABSTRACT

The evolution of galaxies is known to be connected to their position within the large-scale structure and their local environmental density. We investigate the relative importance of these using the underlying dark matter density field extracted from the *Constrained Simulations in* BORG (CSiBORG) suite of *constrained* cosmological simulations. We define cosmic web environment through both dark matter densities averaged on a scale up to 16 Mpc h^{-1}, and through cosmic web location identified by applying DisPerSE to the CSiBORG haloes. We correlate these environmental measures with the properties of observed galaxies in large surveys using optical data (from the NASA-Sloan Atlas) and 21-cm radio data (from ALFALFA). We find statistically significant correlations between environment and colour, neutral hydrogen gas (H I) mass fraction, star formation rate, and Sérsic index. Together, these correlations suggest that bluer, star-forming, H I rich, and disc-type galaxies tend to reside in lower density areas, further from filaments, while redder, more elliptical galaxies with lower star formation rates tend to be found in higher density areas, closer to filaments. We find analogous trends with the quenching of galaxies, but notably find that the quenching of low-mass galaxies has a greater dependence on environment than the quenching of high-mass galaxies. We find that the relationship between galaxy properties and the environmental density is stronger than that with distance to filament, suggesting that environmental density has a greater impact on the properties of galaxies than their location within the larger-scale cosmic web.

Key words: galaxies: evolution – galaxies: statistics – dark matter – large-scale structure of Universe.

1 INTRODUCTION

In the standard model of cosmology, matter evolves from a nearly smooth primordial density field, with small perturbations at the end of the inflationary epoch. These perturbations evolve non-linearly under gravity to form the cosmic web, a tangled structure of nodes, sheets, filaments and voids (Y. B. Zel'dovich 1970).

Nodes consist of galaxy clusters and superclusters and are the most massive, gravitationally bound structures in the Universe. Voids are vast expanses of extremely low density, containing little gas and very few isolated galaxies. Sheets are membrane-like two-dimensional (2D) structures encircling voids. Filaments are long, thread-like structures that form at the intersection of sheets and which connect the nodes. These filaments are made up of galaxies, gas, and dark matter, which can all flow along the filament towards the nodes. In the last decade, a significant amount of work as been undertaken to understand how galaxy evolution is dependent on the position within this cosmic web (e.g. E. Tempel & N. I. Libeskind 2013; Y. Zhang et al. 2015; K. Kraljic et al. 2021; M. N. Tudorache et al. 2022; S. Barsanti et al. 2023).

Moreover, such work can help characterize the relationship between luminous galaxies and the underlying dark matter, which is not directly observable. This is vital for obtaining precision constraints on the cosmological model from forthcoming surveys. The statistics of cosmic web structures are also emerging as a potential test of dark energy, which dominates the late-time evolution of large-scale structure (B. Novosyadlyj & M. Tsizh 2017; P. Boldrini & C. Laigle 2024).

There are a wide variety of proposed mechanisms for how a galaxy's environment may affect properties such as morphology, colour, stellar mass, and metallicity. For example, simulations show haloes of the same mass in different environments have statistically different assembly histories (R. H. Wechsler et al. 2002; A. V. Macciò et al. 2007; P. Behroozi et al. 2019), which should impact the observed baryonic properties (J. Matthee et al. 2017; I. Zehavi et al. 2018; W. Cui et al. 2021). Gas is expected to flow along cosmic filaments, and so galaxies along filaments may be expected to replenish their gas more readily and thus have higher gas content (M. Ramsøy et al. 2021). Spheroidal galaxies are also more commonly located in overdense environments such as nodes and along the filaments, which has been linked to both the age of the most massive haloes and the higher likelihood of galaxy mergers in these dense environments (e.g. T. Naab, P.

★ E-mail: 22c.gallagher@gmail.com

H. Johansson & J. P. Ostriker 2009; M. Cappellari 2016; I. Perez et al. 2025). Galaxy mergers may also lead to quenching, which qualitatively matches the observed higher fraction of red galaxies in denser environments (A. Dressler 1980; Y.-J. Peng et al. 2010; R. J. McLure et al. 2013). The most massive galaxies in the most massive haloes are also more likely to host powerful active galactic nuclei (AGNs) that may suppress star formation on large scales through their powerful jets (R. G. Bower et al. 2006; D. J. Croton et al. 2006; J. Schaye et al. 2015; Y. Dubois et al. 2016; R. G. Bower et al. 2017).

To investigate these effects observationally, large multiwavelength surveys are required, both to map the large-scale cosmic web itself, and then to also measure properties of the galaxies that reside within this structure. In this work we use the NASA-Sloan Atlas (NSA) survey and the Arecibo Legacy Fast Arecibo L-band Feed Array survey (ALFALFA, M. P. Haynes et al. 2018). The NSA is a catalogue of galaxy properties derived from the Sloan Digital Sky Survey (SDSS; D. G. York et al. 2000; K. N. Abazajian et al. 2009; H. Aihara et al. 2011), and contains properties including absolute magnitude, star formation rate (SFR) parameters, metallicity, and stellar mass. ALFALFA is a neutral hydrogen gas (H I) survey. H I is the reservoir of cold gas that condenses to molecular H_2 to form stars (F. Palla, E. E. Salpeter & S. W. Stahler 1983). Therefore, constraining its relationship with galaxy properties is vital for determining the details of galaxy growth. One complication when studying the link between H I and galaxies is that, because H I resides predominantly in the lowest density outer regions of galaxies, it is highly susceptible to environmental effects. In dense environments, H I is often stripped away, as shown by numerous studies (e.g. J. M. Solanes et al. 2001; L. Cortese et al. 2011; K. M. Hess & E. M. Wilcots 2013; M. C. Odekon et al. 2016).

Throughout the literature, the three-dimensional (3D) cosmic web structure is identified observationally by applying a variety of structure-finding algorithms (N. I. Libeskind et al. 2018) to large-scale spectroscopic galaxy surveys such as the Sloan Digital Sky Survey (SDSS), from which the 3D positions of galaxies can be extracted. By analysing the distribution of the galaxies in these surveys, it is also possible to estimate the density of matter in different regions of space (E. Tempel et al. 2014), or to measure proxy statistics such as distance to nearest neighbour. However, methods based on galaxy catalogues suffer from survey incompleteness and uncertainty in galaxy distances. The most desirable way to define the cosmic web would be to use the underlying dark matter density field. Modern dark matter-only cosmological simulations can be used to calculate the cosmic web very precisely (R. E. Angulo & O. Hahn 2022). However, most *N*-body simulations use initial conditions with random phases of density fluctuations in the early Universe, producing structure that resembles the actual Universe only statistically.

In this work, we instead use *constrained* simulations, which enable the encoding of both the amplitude and phases of the primordial density perturbations, giving the full 3D density and large-scale structure fields. Other key projects using constrained simulations include the ELUCID project (H. Wang et al. 2016a; X. Yang et al. 2018; Y. Zhang, X. Yang & H. Guo 2022; X. Xu et al. 2024), which investigates the relationship between constrained simulations and the SDSS, and the CLUES collaboration (S. Gottloeber, Y. Hoffman & G. Yepes 2010; J. G. Sorce et al. 2016) which aims to reconstruct the local universe and its clusters. The CLUES project uses the Weiner-filter method to reconstruct the mean field, but does not provide uncertainty quantification. Here, we adopt the *Constrained Simulations in* BORG (CSiBORG) suite (D. J. Bartlett, H. Desmond & P. G. Ferreira 2021; D. J. Bartlett et al. 2022; H. Desmond et al. 2022; M. L. Hutt et al. 2022; A. Kostić, D. J. Bartlett & H. Desmond 2023; R. Stiskalek et al. 2024, 2025), based on the Bayesian Origin Reconstruction from Galaxies (BORG) algorithm (J. Jasche & B. D. Wandelt 2013; J. Jasche, F. Leclercq & B. D. Wandelt 2015; F. Leclercq 2015; G. Lavaux & J. Jasche 2016; J. Jasche & G. Lavaux 2019; L. Doeser et al. 2024; S. Stopyra et al. 2024). The BORG algorithm is a Bayesian forward modelling algorithm that works as follows: it evolves the dark matter density field from initial conditions with some set of phases. The dark matter field is then populated with galaxies according to some galaxy bias model (relating dark matter and galaxy distribution), and a selection function corresponding to the relevant survey applied. The model galaxy field is then compared to observations through a likelihood, and the initial phases constrained through Bayesian inference. These phases are then used as initial conditions in CSiBORG, leading to a suite of 101 *N*-body simulations, corresponding to samples from the posterior. Hence, the BORG algorithm ensures that the large-scale structure in the CSiBORG simulations is positioned such that it matches the actual distribution of cosmic web structure in the Universe (J. Jasche & G. Lavaux 2019).

In this study, we define a galaxy's cosmic web environment in two ways: the first using the dark matter density at the position of the galaxy as given by CSiBORG (smoothed on some scale), and the second by calculating the distance of the galaxy from the filaments and nodes of the cosmic web, which are found by applying the Discrete Persistence Structure Extractor algorithm (DisPerSE; T. Sousbie, C. Pichon & H. Kawahara 2011a, b) directly to the CSiBORG dark matter haloes. It should be noted that, in our first definition, galaxies are not assumed to lie at halo centres; the dark matter density is evaluated at the observed galaxy position in the smoothed CSiBORG field. By using constrained simulations to quantify cosmic web environment, we aim to measure the strength of correlations between a galaxy's environment and the properties of its gas and stars, which will constrain the relative importance of different galaxy formation processes. We aim to differentiate between those effects caused by the position of a galaxy relative to the 3D cosmic web structure, and those effects caused by the local dark matter density. Importantly, the fact that CSiBORG is a suite of simulations spanning the posterior of the BORG inference, means that we are able to propagate uncertainties in our knowledge of the dark matter field of the local Universe into our galaxy–environment correlation statistics. This affords, for the first time, a quantitative assessment of their statistical significance.

This paper is structured as follows: Section 2 details the data used, including CSiBORG, NSA, and ALFALFA. Section 3 details the methodology used to find correlations, define the structure of the cosmic web, smooth the CSiBORG fields and define quenching. Section 4 presents the results and Section 5 discusses their interpretation and comparison with the literature. Finally, Section 6 concludes with a summary of our findings.

2 OBSERVED AND SIMULATED DATA

We use simulation data from CSiBORG, and galaxy properties from the NSA and ALFALFA surveys. The galaxy SFRs are obtained from the Max Planck Institute for Astrophysics/John Hopkins University (MPA/JHU) survey. The properties of galaxies used throughout this report are summarized in Table 1. The effective volume and number of galaxies of each sample of data can be found in Table 2.

Table 1. Summary of quantities used in this work, including galaxy properties which we correlate with their environment, and the dark matter density from CSiBORG. ρ_0 denotes the unsmoothed density field, which has a spatial resolution of 0.66 Mpc h^{-1}.

Quantity	Units	Description	Source Catalogue
$M_\star$	$M_\odot$	Total stellar mass of a galaxy.	NSA
Colour	Magnitudes	$u-r$ band.	NSA
Sérsic index	–	2D Sérsic index, quantifying the concentration of a galaxy's light profile.	NSA
Metallicity	–	Metallicity from k-correction fit.	NSA
Size	Arcsec	Angular effective radius (Petrosian 50 per cent light radius).	NSA
$M_{\rm HI}/M_\star$	–	The neutral hydrogen mass fraction of a galaxy, i.e. the total mass of H I in a galaxy divided by its total stellar mass.	ALFALFA
SFR	$M_\odot\,{\rm yr}^{-1}$	The instantaneous SFR of a galaxy.	MPA/JHU
sSFR	$1\,{\rm yr}^{-1}$	The instantaneous sSFR of a galaxy (SFR/$M_\star$).	MPA/JHU
ρ_σ where $\sigma = 0, 2, 4, 8, 16$	$h^2 M_\odot\,{\rm kpc}^{-3}$	The dark matter density field smoothed on a scale σ in units of Mpc h^{-1}.	CSiBORG

Table 2. The number of galaxies ($N_{\rm gal}$) and effective volume ($V_{\rm eff}$) for each sample in 10^6 Mpc^3, after cross-matching data sets and restricting to the CSiBORG high-completeness region. The effective volume was calculated using a voxel-based method applied to the 3D galaxy positions of the NSA-CSiBORG sample, and then inferred for the subsequent samples by assuming ratio of galaxies lost approximately corresponds to the fraction of volume lost.

Sample	$N_{\rm gal}$	$V_{\rm eff}[10^6{\rm Mpc}^3]$
NSA	641 409	–
NSA-CSiBORG	89 328	2.2
NSA-CSiBORG-MPA/JHU	81 281	2.0
ALFALFA	31 500	–
NSA-CSiBORG-ALFALFA	22 478	0.56
NSA-CSiBORG-ALFALFA-MPA/JHU	16 276	0.40

2.1 Simulation data

Introduced in D. J. Bartlett et al. (2021), the CSiBORG suite comprises 101 N-body simulations. Spanning a three-dimensional box with dimensions of 677.7 Mpc h^{-1}, centred on the Milky Way, these simulations use initial conditions inferred from the Bayesian Origin Reconstruction from Galaxies algorithm (BORG; J. Jasche & B. D. Wandelt 2013; J. Jasche et al. 2015; F. Leclercq 2015; J. Jasche & G. Lavaux 2019; L. Doeser et al. 2024; S. Stopyra et al. 2024) applied to the 2M++ galaxy survey (G. Lavaux & M. J. Hudson 2011), which has a high completeness within a spherical region of radius 155 Mpc h^{-1} centred on the Milky Way. Specifically, this version of CSiBORG is based on the initial conditions presented in J. Jasche & G. Lavaux (2019).

The 2M++ reconstruction encompasses a cubic volume with a side length of 677.7 Mpc h^{-1} divided into 256^3 voxels, resulting in a spatial resolution of 2.65 Mpc h^{-1}. Similarly, CSiBORG features a high-resolution sphere centred on the Milky Way, with a radius of 155 Mpc h^{-1}. In this region, initial conditions are augmented with white noise to account for random fluctuations on subconstraint scales. The spatial distribution is defined on a grid measuring 2048^3, yielding an initial interparticle spacing of 0.33 Mpc h^{-1}. Surrounding this high-resolution region, there is a spherical buffer zone with a width of 10 Mpc h^{-1}, ensuring a smooth transition to the base BORG resolution. Fig. 1 shows a slice of the CSiBORG box at different degrees of Gaussian smoothing (see Section 3.1). The three plots are zoomed in on the central region of high completeness. The left panel clearly shows a cross-section of the central spherical high-completeness region.

Dark matter haloes are identified as in R. Stiskalek et al. (2024): within the central high-completeness region, the friends-of-friends halo finder (FOF; M. Davis et al. 1985) is used, with a linking-length parameter of $b = 0.2$. The FOF algorithm connects particles within a distance b times the mean particle separation. We require a minimum of 100 particles for a halo, corresponding to a minimum halo mass of $3.09 \times 10^{11} M_\odot\,h^{-1}$.

The dark matter density field is reconstructed from $z = 0$ particle snapshots. To convert them into a continuous density field, we employ the smoothed-particle hydrodynamics method (J. J. Monaghan 1992; S. Colombi, M. J. Chodorowski & R. Teyssier 2007). As outlined in Section IV.B.1 of D. J. Bartlett et al. (2022), a minimum of 32 neighbouring particles is required to smooth over. The resulting density field is then mapped onto a grid with a resolution of 0.7 Mpc h^{-1}. Both BORG and CSiBORG adopt the following cosmological parameters: $T_{\rm CMB} = 2.738$ K, $\Omega_m = 0.307$, $\Omega_\Lambda = 0.693$, $\Omega_b = 0.04825$, $H_0 = 70.05\,{\rm km\,s^{-1}\,Mpc^{-1}}$, $\sigma_8 = 0.8288$ and $n = 0.9611$. Lastly, for the purpose of this work we also use 20 CSiBORG-like simulations but with random initial conditions to produce density fields that are uncorrelated with the observed galaxy properties.

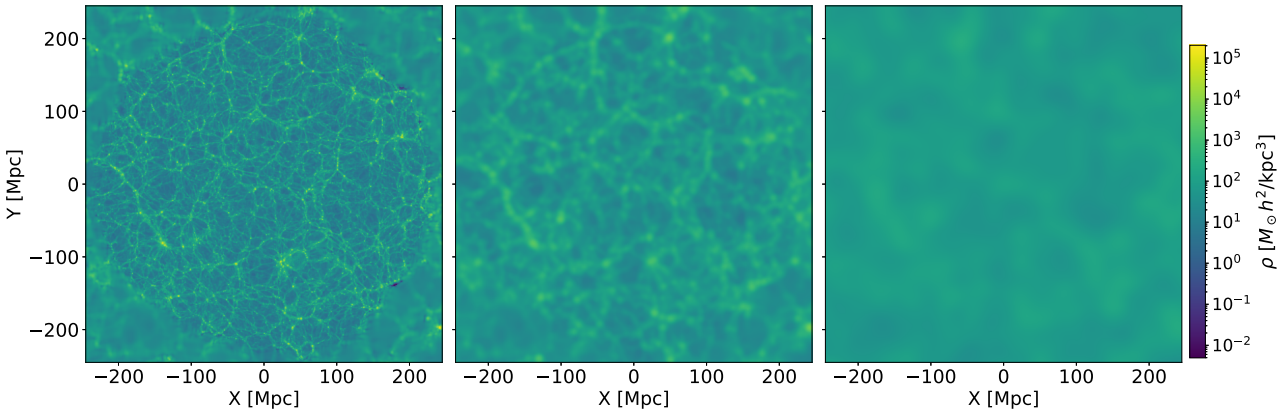

Figure 1. The dark matter distribution from a single realization of CSiBORG, shown without and then with Gaussian smoothing of standard deviation $\sigma = 2$ and 8 Mpc h^{-1} (middle and right panel). Each panel represents a 2D slice through the Z-axis of the simulation box, centred on the Milky Way. The high-completeness central region of radius 155 Mpc h^{-1} is visible. As smoothing increases the smaller scale structures are smoothed out. See Section 2.1 for further details of CSiBORG, and Section 3.1 for further details of the smoothing methodology.

2.2 Nasa-Sloan Atlas

We use the NSA survey[1] to obtain galaxy properties such as the stellar mass ($M_\star$), colour ($u - r$), Sérsic index, size, and metallicity. A summary of these properties is provided in Table 1. However, it should be noted that the correlations with metallicity and stellar mass, presented in Section 4, should be used with caution, as stated explicitly in the NSA data base.

The NSA data base contains images and parameters of local galaxies, based on SDSS DR8 (H. Aihara et al. 2011) and the Galaxy Evolution Explorer survey (GALEX; D. C. Martin et al. 2005). We used the nsa_v1_0_1 data[2], which has a redshift range out to $z = 0.15$ and contains approximately 640 000 galaxies.

The distribution of these galaxies is illustrated in the right-hand panel in Fig. 2. After restricting the NSA sample to the region covered by 2M++, which was used to constrain the CSiBORG density field, we obtain a total of approximately 90 000 galaxies at a redshift of $z \leq 0.05$.

We obtain data for the SFR and specific star formation rate (sSFR) of galaxies from MPA-JHU catalogue[3], which is based on G. Kauffmann et al. (2003); J. Brinchmann et al. (2004); C. A. Tremonti et al. (2004). This catalogue is part of data release 8 of the SDSS, and provides derived galaxy properties based on spectral measurements.

2.3 ALFALFA

The ALFALFA[4] survey maps nearly 7000 deg^2 of high galactic latitude sky using the Arecibo telescope, obtaining HI 21 cm line measurements for 31500 galaxies out to a redshift of 0.06 (M. P. Haynes et al. 2018). We use the ALFALFA galaxy HI masses.

We use an NSA and ALFALFA cross-match to obtain the $M_\star$, colour, SFR, Sérsic index, size and HI corresponding to ALFALFA galaxies. We match the NSA and ALFALFA catalogues by using a method following R. Stiskalek et al. (2021), exploiting the partial overlap between ALFALFA and SDSS. This method matches the optical counterpart position to the sources in the NSA using an on-sky angle tolerance and line-of-sight tolerance of 5 arcsec and 10 Mpc, respectively. This constitutes a strict criteria ensuring a low likelihood of mismatches and high sample purity. This cross-match retains approximately 22000 galaxies. Due to the flux-density limit of ALFALFA, there is a relatively steep Malmquist bias with redshift for the H I-detected galaxies. Furthermore, the galaxies in this ALFALFA-NSA data set are bluer in colour than those from the general NSA galaxy sample, with higher SFRs. This is expected, given the selection of galaxies rich in HI. Consistent with this, we also find in this sample a clear correlation between SFR and $M_{\rm HI}$. The sky distribution of galaxies can be seen in the left-hand plot of Fig. 2.

[1] http://nsatlas.org/data
[2] https://www.sdss4.org/dr17/manga/manga-target-selection/nsa/
[3] https://www.sdss4.org/dr17/spectro/galaxy_mpajhu/
[4] http://egg.astro.cornell.edu/alfalfa/data/index.php

3 METHODOLOGY

3.1 Density statistics

We begin by defining statistics of the dark matter density field, which we then correlate with galaxy properties. We do this as follows. We conduct our analysis using 101 realizations of the CSiBORG simulations from which we obtain the dark matter density fields $\rho_{\rm DM}$. For every realization, we use the 'native' SPH density field (ρ_0) along with four realizations of the field smoothed at different scales (ρ_d for $d = 2,\ 4,\ 8,\ 16$ Mpc h^{-1}). We choose these degrees of smoothing in order to provide insights across a large range of spatial scales. We then correlate these with the galaxy properties in Table 1. This allows us to investigate the effect of different spatial scales on various astrophysical processes. The Gaussian smoothing operates such that for a function $\rho(\boldsymbol{r})$, then

$$\rho_{\rm smoothed}(\boldsymbol{r}) = \frac{1}{\sigma^3(2\pi)^{\frac{3}{2}}} \int_{\mathcal{R}} \rho_{\rm DM}(\boldsymbol{r}') \exp\left(\frac{|\boldsymbol{r} - \boldsymbol{r}'|^2}{2\sigma^2}\right) \mathrm{d}\boldsymbol{r}', \qquad (1)$$

where σ is the standard deviation of the Gaussian smoothing kernel in units of Mpc h^{-1}. The smoothed dark matter density field is rendered on a 1024^3 grid such that the baseline of 'no additional smoothing' has a spatial resolution of 0.66 Mpc h^{-1} . This approximately corresponds to the typical scale of a cluster-sized halo (N. A. Bahcall 1999). Note however that the constraints on the initial conditions are on a 2.6 Mpc h^{-1} scale, and hence

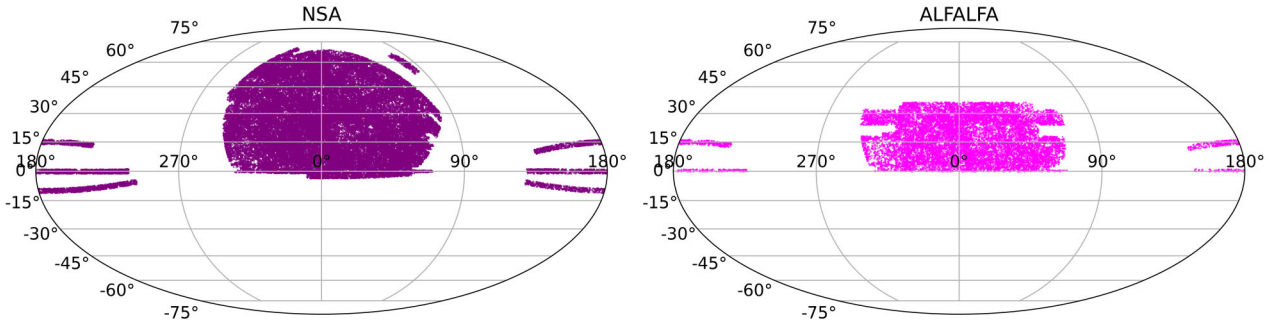

Figure 2. The distribution of NSA galaxies (left) and ALFALFA galaxies (right), shown on Mollweide projections of right ascension and declination. The NSA catalogue, based on optical data, contains information for 640 000 galaxies out to a redshift of 0.15. The ALFALFA catalogue provides HI 21 cm line measurements for 31 500 galaxies out to a redshift of 0.06, covering nearly 7000 deg^2 of high galactic latitude sky. See Sections 2.2 and 2.3 for further information on the NSA and ALFALFA surveys respectively.

below this there is limited information on the actual density field. Fig. 1 shows a 2D slice of a single CSiBORG realization of the dark matter density field for ρ_0, ρ_2, and ρ_8. The effect of Gaussian smoothing can be seen on these plots, which show how finer features become more blurred as smoothing increases.

Estimating the dark matter density at the galaxy position should take into account its distance uncertainty. The NSA catalogue provides distances calculated using the Willick flow model (J. A. Willick et al. 1997), however no uncertainty is provided. The expected typical distance uncertainty due to small-scale velocities not accounted for by the model, is ~ 300 km s^{-1} (R. Stiskalek et al. 2025), which corresponds to a distance uncertainty of ~ 3 Mpc h^{-1}. Therefore even our smallest smoothing scale should smooth out variations in the dark matter density comparably to the distance uncertainty (and the 2.6 Mpc h^{-1} scale of the initial condition constraints).

3.2 Cosmic web statistics

To define the cosmic web we use the Discrete Persistence Structure Extractor[5] algorithm (DisPerSE; T. Sousbie et al. 2011a, b), which uses discrete Morse theory (J. W. Milner 1963) to detect topological features: maxima, minima and saddle points. These features can then be used to convert the density field into the structural elements of the cosmic web: nodes, filaments, sheets, and voids.

DisPerSE can be applied to any discrete point distribution and is most commonly used in observational studies on galaxy catalogues. However, our use of constrained simulations enables us to apply it directly to the dark matter at either the particle or halo level, sidestepping issues associated with galaxy bias. We choose to apply it to the halo catalogues rather than particle data because this approach has been tested and calibrated by D. Galárraga-Espinosa et al. (2024). In that work, the DisPerSE parameters were calibrated for halo catalogues to maximize the purity and completeness of associating nodes with the positions of massive haloes in non-constrained simulations. We outline their method and parameter choices below. We apply DisPerSE to all 101 realizations of CSiBORG dark matter haloes, along with 20 unconstrained simulations to allow us to determine the statistical significance of our results (see Section 4).

[5] https://www2.iap.fr/users/sousbie/web/html/indexd41d.html

The DisPerSE algorithm starts by constructing a 3D Delaunay tessellation field, using the Delaunay Tessellation Field Estimator (DTFE; W. E. Schaap & R. van de Weygaert 2000). The DTFE density field is estimated directly from halo positions without applying halo-mass weights, as in D. Galárraga-Espinosa et al. (2024). We use periodic boundary conditions to estimate the particle density field. We then apply the 'netconv' smoothing function to this density field, taking the smoothing threshold value as 1σ. We then apply the 'mse' function, which is the 'manifold skeleton extractor' and the primary function of DisPerSE. This identifies the critical points of the density field and requires the user to input a persistence threshold, which we take to be 2σ. This threshold is important as if it is too low, it may lead DisPerSE to map noise as filaments, or if too high, DisPerSE may miss the finer structures.

The values that we take for smoothing and persistence threshold are consistent with D. Galárraga-Espinosa et al. (2024), who look for the optimal smoothing and persistence threshold parameters that recover the most accurate cosmic web features while minimizing noise. We then apply the 'skelconv' function to convert the outputs into a readable format, with critical points indicating when the gradients of the manifold are equal to zero. The critical points are maxima, minima, and saddle points. The filament arms are given by connecting a maxima to a saddle point and are made up of many small segments. The filament distribution overlaid on one realization of the dark matter haloes, alongside the observational data, is shown in Fig. 3.

With the filament locations identified, we calculate the midpoint of each segment, and compare these with the galaxy coordinates from the NSA data base, in order to compile a list of the 'distance to the nearest filament' for every galaxy, which we hereafter refer to as $\mathrm{d_{fil}}$. As the average segment size is about 1 Mpc, the error from the discretization of the filament is negligible. The process produces 101 separate sets of $\mathrm{d_{fil}}$, each corresponding to a realization of the CSiBORG dark matter haloes. Additionally we obtain 20 sets of $\mathrm{d_{fil}}$ corresponding to the unconstrained simulations.

3.3 Correlation statistics

We use two methods to calculate the correlation between data sets: a direct Spearman correlation between two properties ('direct correlation'), and a partial Spearman correlation conditioned on $M_\star$, ρ_{DM}, or $\mathrm{d_{fil}}$ ('partial correlation').

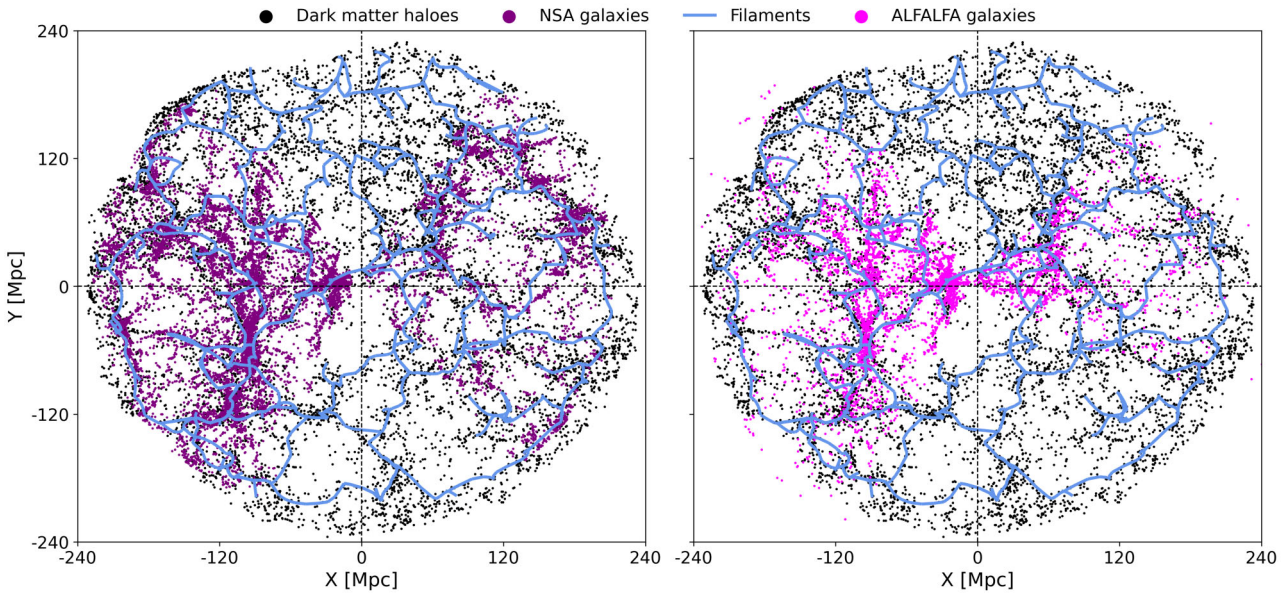

Figure 3. Distribution of dark matter haloes (black) derived from CSiBORG, overlaid with NSA galaxies (purple; left panel), ALFALFA galaxies (magenta; right panel) and cosmic web filaments (blue), shown in a 15 Mpc slice along the z-axis centred on the Milky Way. The cosmic web filaments are calculated using DisPerSE, applied to the CSiBORG haloes. NSA and ALFALFA galaxies predominantly cluster along the filamentary structures, with some galaxies distributed within the voids of the cosmic web. See Section 2.1 for details on the CSiBORG haloes, and Section 3.2 for further details on the DisPerSE methodology and filament extraction.

The Spearman rank correlation coefficient quantifies whether a relation between two variables can be described by a monotonic function. Unlike the Pearson correlation coefficient, which measures linear relationships, the Spearman correlation coefficient takes into account the ranks of the data points rather than their raw values. Therefore, it is less sensitive to outliers, since outliers have a smaller effect on the ranking of the data. The Spearman correlation coefficient is calculated by considering n pairs of observations from two distributions, with the observations in each distribution ranked from smallest to largest (M. G. Kendall & A. Stuart 1973). Then, if d_i is the difference between the ranks of each observation, the Spearman rank correlation coefficient, r_S, is given by

$$r_S = 1 - \frac{6\sum d_i^2}{n(n^2-1)}. \quad (2)$$

We also use a partial correlation method to quantify the relationship between a galaxy property and either $\rho_{\rm DM}$ or $\mathrm{d_{fil}}$, while controlling for a third property: $M_\star$, $\rho_{\rm DM}$ or $\mathrm{d_{fil}}$. This is achieved by fitting a locally weighted scatter plot function (LOWESS[6]; W. S. Cleveland 1979) between each variable of interest (A and B) and the third property (C, the condition). LOWESS fits a generalized non-linear function to the data, by locally fitting a weighted least squares regression line. We use LOWESS as it handles outliers more reliably than a basic curve fit function, and allows for flexibility in the fit when handling complex data with a non-trivial relationship. We then compute the residuals from the fit between A and C, and then between B and C. The Spearman rank correlation coefficient is calculated between the two sets of residuals, providing the partial correlation between A and B, conditioned on property C.

Where there is a bimodal relationship between a variable and stellar mass, we separate the two distributions. For example, with colour, SFR, and sSFR we separate 'quenched' and 'star-forming' galaxies in line with the process later described in Section 3.4 and visible in Fig. 5. We find the residuals of these distributions separately. Fig. 4 shows how the residuals were found for colour, after splitting the bimodal colour distribution as star-forming or quenched galaxies.

We apply the above procedure to extract the correlation coefficients between galaxy and environmental properties ($\rho_{\rm DM}$ and $\mathrm{d_{fil}}$) for the 101 constrained simulations as well as the 20 unconstrained simulations. We find that for the unconstrained simulations, the distributions of correlation coefficients are approximately Gaussian and centred on zero. We find that the standard deviations of the distributions are much smaller for the constrained simulations than the unconstrained simulations, showing the uncertainty due to the BORG posterior is small. We perform bootstrapping with replacement to test the uncertainty due to the finite sample size of the galaxy surveys, but find it is negligible.

Given the above, we quantify the statistical significance of each correlation as the mean of the correlation coefficients from the constrained simulations divided by the standard deviation of the coefficients from the unconstrained simulations. This tests against the null hypothesis of no correlation between environment and any of the galaxy properties, which is necessarily the case in the unconstrained simulations.

3.4 Quenched fraction

We also study the dependence of the quenched fraction of galaxies on $\rho_{\rm DM}$ and $\mathrm{d_{fil}}$. In Fig. 5 we plot the SFR (from the MPA/JHU

[6] https://www.statsmodels.org/dev/generated/statsmodels.nonparametric.smoothers_lowess.lowess.html

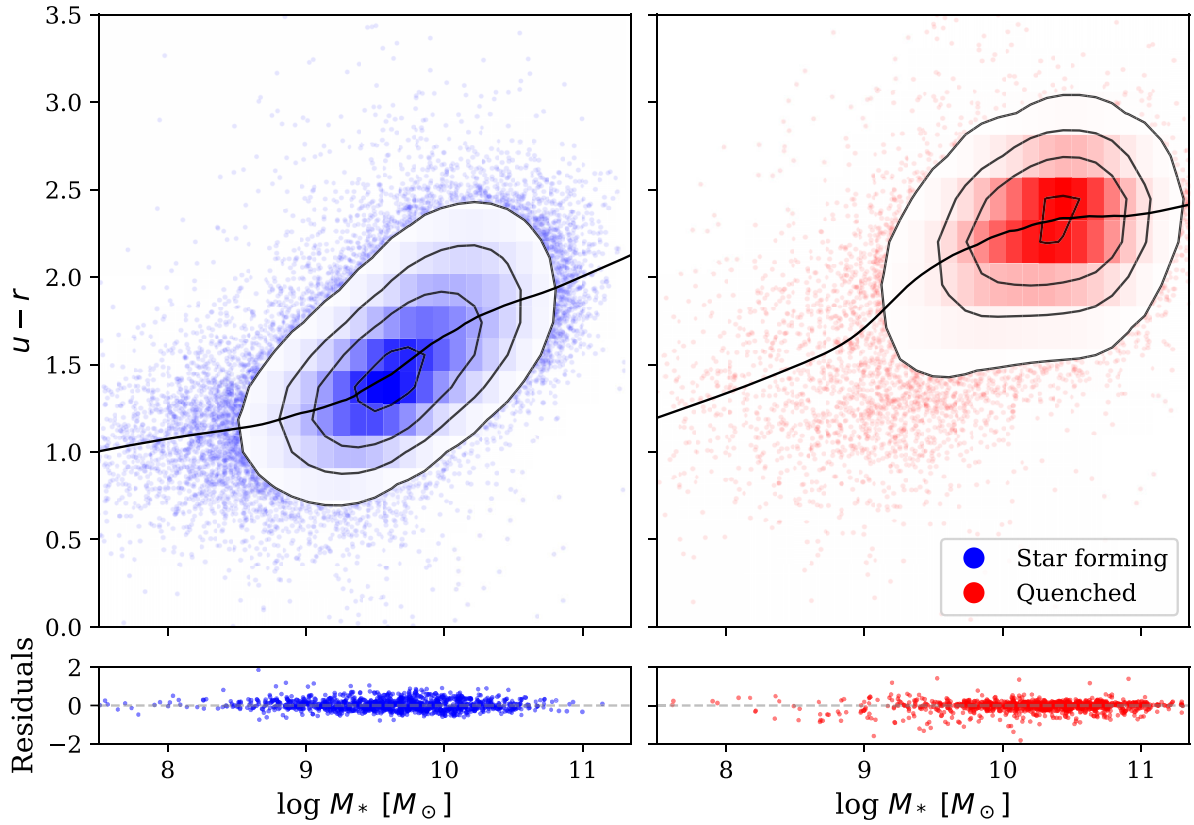

Figure 4. The relationship between colour ($u - r$) and stellar mass, with the solid black line showing the LOWESS fit. The bimodal distribution of colour has been separated into 'star-forming' (left) and 'quenched' (right). The contour lines show the points contained within 0.5σ, 1σ, 1.5σ, and 2σ, which represents 11.8 per cent, 39.3 per cent, 67.5 per cent, and 86.4 per cent regions of each distribution, respectively.

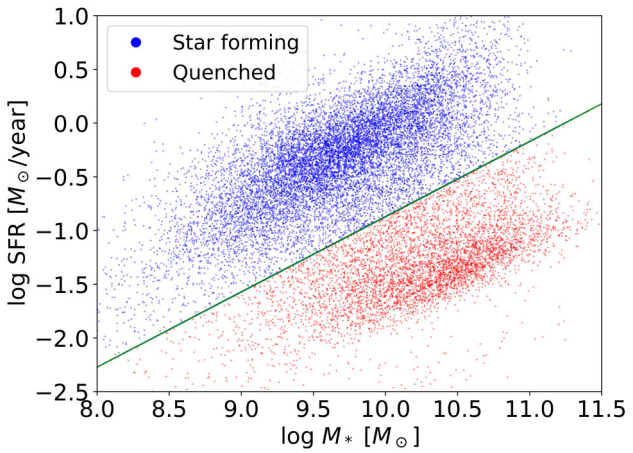

Figure 5. The bimodal distribution of the SFR of NSA galaxies (from the MPA/JHU catalogue), classifying galaxies as star-forming (blue; above the dividing line) and quenched (red; below the dividing line). We use equation (3) to divide the two populations. See Section 3.4 for further details on the methodology of defining a quenched galaxy.

catalogue) against $M_\star$, which produces a bimodal distribution of galaxies. This can be split into galaxies on the 'main sequence', which we define as star forming, and those below this main sequence band, which we define as quenched.

We define galaxies as star forming or quenched with the following definition of the main sequence from K. E. Whitaker et al. (2012):

$$\log_{10}(\mathrm{SFR}/\mathrm{M}_\odot\ \mathrm{yr}^{-1}) = \alpha(z)[\log_{10}(M_\star/\mathrm{M}_\odot) - 10.5] + \beta(z), \quad (3)$$

where the slope $\alpha(z) = 0.70 - 0.13z$ and the normalization factor $\beta(z) = 0.38 + 1.14z - 0.19z^2$. We then subtract 1 dex from $\log_{10}(\mathrm{SFR})$ in order to find the line separating the star forming and quenched sequences, as this is approximately at the minima between the star formation main sequence and the population of quenched galaxies.

4 RESULTS

Here we present the results obtained for the relationship of galaxy properties (described in Table 1) with environmental density ρ_{DM} and distance from filament $\mathrm{d_{fil}}$. For simplicity, we will henceforth refer to the ALFALFA×NSA data as 'ALFALFA data'. For a direct comparison between the results presented here and the corresponding literature, please see Sections 5.1 and 5.2.

In Fig. 6, we show the relationship between dark matter density and distance from filament (inferred from `CSiBORG`) evaluated at the position of NSA galaxies. As expected, there is a strong anticorrelation between mean density and distance to filament. To fully investigate the relative effect of filament distance and density on galaxy properties, we study their correlations with

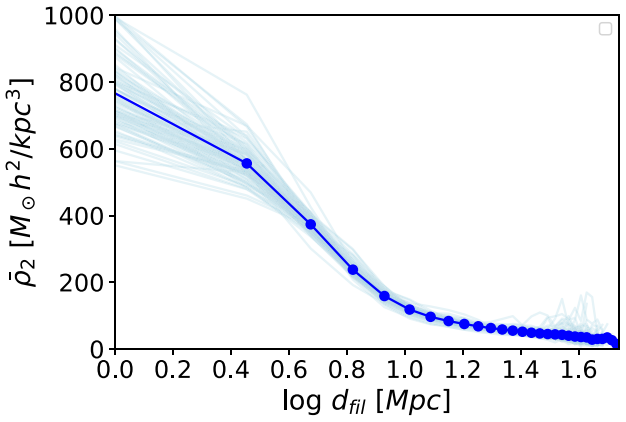

Figure 6. The relationship between the matter density ρ_2 and distance to nearest filament d_{fil} evaluated at the position of NSA galaxies. The thin lines are the relations inferred from individual CSiBORG realizations, whereas the bold blue is their mean. ρ_2 rapidly decreases with d_{fil}, affirming that the dark matter density is concentrated around the filament, and that there is a sharp density gradient surrounding the filament.

ρ_{DM} and d_{fil} individually, as well as their correlation with ρ_{DM} conditioned on d_{fil} and vice versa.

4.1 NSA correlations

The results for the Spearman correlations of galaxy properties taken from the NSA survey (see Table 1) with ρ_{DM} and d_{fil} are shown in the top and bottom rows of Fig. 7. This figure shows the direct correlation between galaxy properties with ρ_{DM} and d_{fil} in the top left panel, the partial correlation conditioned on $M_\star$ between galaxy properties with ρ_{DM} and d_{fil} in the top right panel, the partial correlation between galaxy properties and ρ_{DM} conditioned on d_{fil} in the bottom left panel, and the partial correlation with d_{fil} conditioned on ρ_{DM} in the bottom right panel. We show the uncertainty, or 'statistical significance' of each correlation in parentheses below the value of the correlation, with a description of how this was calculated in Section 3.3.

The direct correlations of both ρ_{DM} and d_{fil} with galaxy properties (colour, SFR, sSFR and Sérsic index) are statistically significant. For ρ_{DM}, the correlation peaks around ρ_0 or ρ_2, generally showing stronger correlations than those for d_{fil}, with comparable or higher statistical significance (e.g. correlation coefficient of -0.13 with statistical significance 8σ for ρ_2 with sSFR, compared to 0.10 and statistical significance 6σ for d_{fil}). When conditioned on stellar mass, size displays stronger correlations with ρ_{DM} than the direct correlation. Notably, conditioning on d_{fil} yields stronger correlations than conditioning on ρ_{DM}.

There is a notably weak correlation between $M_\star$ and ρ_{DM} with a low statistical significance. We tested this by defining a set of high-mass galaxies ($M_\star > 10^{10.5}M_\odot$) and finding the fraction of high-mass galaxies in bins of ρ_{DM}. The right-hand panel of Fig. 8 shows this fraction as a function of density: we can see that high-mass galaxies tend to be found in denser environments. Y. Wang et al. (2025) study the dependence of galaxy luminosity functions on environment, for different density bins. Their Fig. 2 shows that at the faint end of the luminosity function, the number density of galaxies is nearly independent of environment. At the bright end, however, the number density is reduced in low-density environments compared to high-density regions. This supports the idea that high-mass galaxies tend to reside in higher density environments, and suggests that low-mass galaxies are scattered across all environmental densities. It is likely that the more scattered distribution of low-mass galaxies washes out the correlation between $M_\star$ and ρ_{DM}, hence why we see a very low correlation between $M_\star$ and ρ_{DM} in Fig. 7.

4.2 ALFALFA correlations

Next, we investigate the correlation between ρ_{DM} and d_{fil} with galaxy properties for the ALFALFA galaxies. In addition to the galaxy properties investigated for the NSA data, we also include the $M_{HI}/M_\star$. The correlation results are presented in the middle row of Fig. 7, with the direct correlation in the left panel, and the partial correlation conditioned on $M_\star$ in the right panel.

The direct correlation for the ALFALFA data reveals statistically significant negative correlations between $M_{HI}/M_\star$ and ρ_{DM}, with the strongest correlation and peak statistical significance with ρ_4. The ALFALFA partial correlation conditioned on $M_\star$ reveals very weak correlations of low statistical significance across all galaxy properties. The highest statistical significance is 2σ for the correlations with colour. The ALFALFA partial correlations conditioned on $M_\star$ between any property and d_{fil} are weak and of low statistical significance.

The weak correlations displayed by the ALFALFA galaxy properties are likely due to the selection effects of the ALFALFA survey, which contains preferentially bluer, star-forming galaxies, as these tend to be H I rich. This selection results in a narrower range of galaxy properties, reducing the observed correlation strengths. Additionally, the smaller sample size of the ALFALFA data set likely contributes to the weak correlations and low statistical significance.

4.3 Galaxy quenching

We now investigate the relationship between the dark matter density, distance to nearest filament and the quenching of galaxies in the NSA catalogue. We test this separately for low- and high-mass galaxies, as previous studies suggest that quenching mechanisms can depend on galaxy mass (A. F. L. Bluck et al. 2014; P. H. Goubert et al. 2024; Y. Zheng et al. 2025). Following P. H. Goubert et al. (2024), we define a high-mass galaxy as $M_\star > 10^{10.5}M_\odot$.

Fig.9 shows the correlation between ρ_{DM} and the fraction of quenched galaxies across different smoothing scales. The solid lines represent the average correlation (mean of 101 realizations of CSiBORG) as a function of smoothing scale for high-mass (red) and low-mass (blue) galaxies. The shaded area shows the standard deviation across the 101 realizations.

The correlation between the fraction of quenched galaxies and ρ_{DM} is stronger for low-mass galaxies than for high-mass galaxies. For both high- and low-mass galaxies, the correlation decreases while smoothing scale increases. The standard deviation increases towards ρ_{16} (particularly for the low-mass galaxies), likely due to the fact that the result becomes increasingly randomized as the scale becomes less relevant. Following the split, we have $\sim 76\,000$ and $\sim 13\,000$ low- and high-mass galaxies, respectively, thus the standard deviation in the correlation coefficient of high-mass galaxies is larger.

Lastly, Fig. 10 shows how the fraction of quenched galaxies changes with d_{fil} and ρ_2. We choose ρ_2 for this analysis, as this scale produces the greatest statistical significance for the majority of the correlations in Fig. 7. We see a stronger correlation between

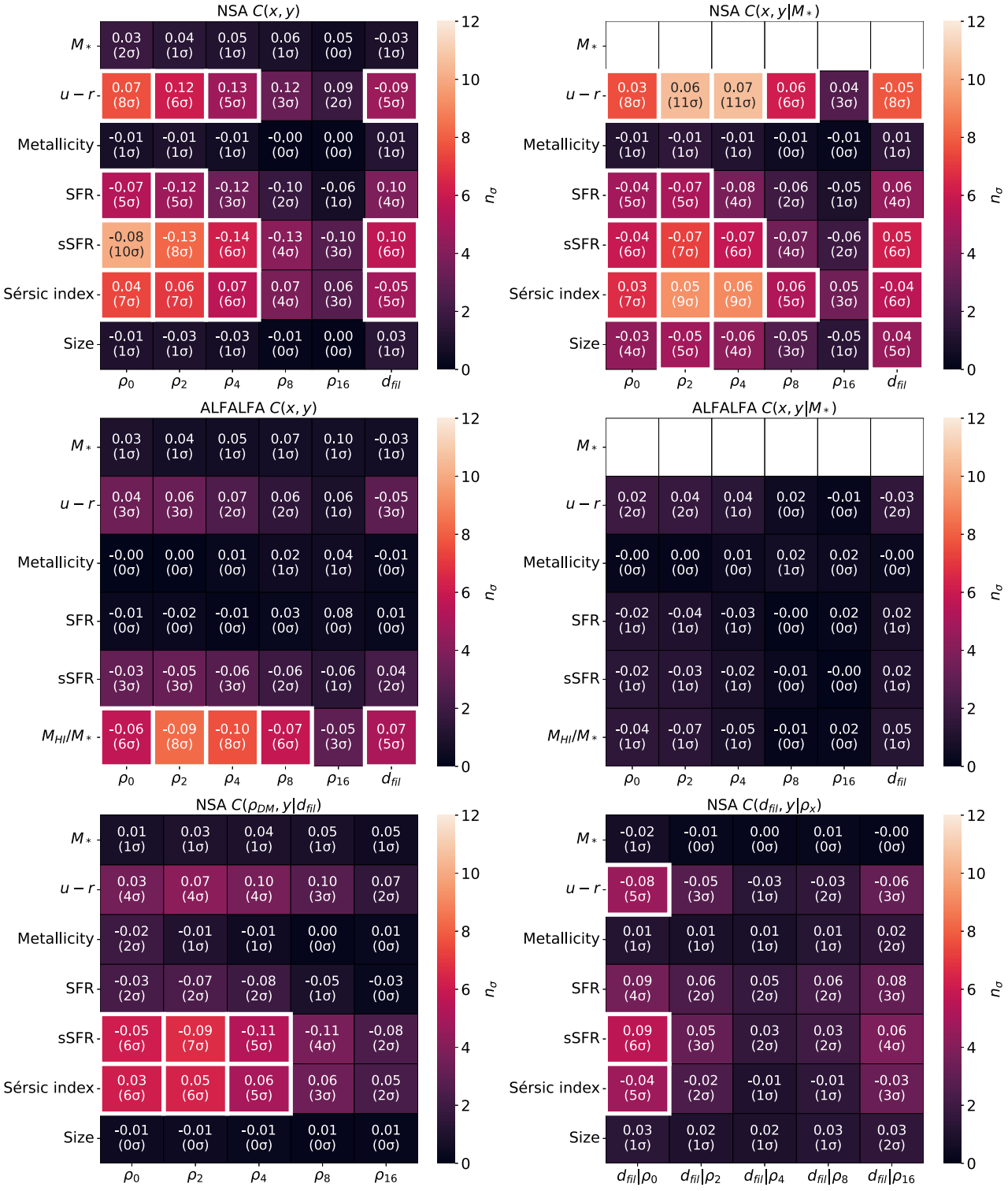

Figure 7. Correlation coefficients of galaxy properties with $\rho_{\rm DM}$ and $\rm d_{fil}$, along with the associated uncertainty and statistical significance of the correlation given in brackets.
A white box indicates a correlation of at least 5σ statistical significance. The first row shows the direct correlation (left) and partial correlation conditioned on $M_\star$ (right) between NSA galaxy properties and $\rho_{\rm DM}$ or $\rm d_{fil}$. The second row shows the same correlations for ALFALFA galaxies. The third row shows the partial correlation between NSA galaxy properties and $\rho_{\rm DM}$ conditioned on $\rm d_{fil}$ (left), and the partial correlation between NSA galaxy properties and $\rm d_{fil}$ conditioned on $\rho_{\rm DM}$ (right). Correlations of galaxy properties with the dark matter density are typically stronger than those with the filament distance. See Sections 4 and 5.1 for a description and interpretation of these results, respectively.

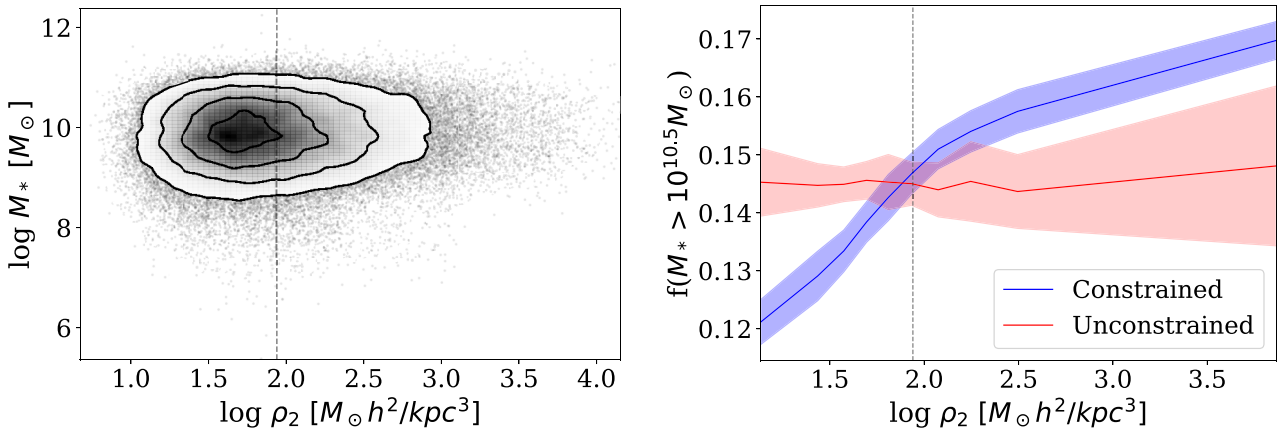

Figure 8. The relationship between dark matter density ρ_2 and stellar mass $M_\star$ (left) and the fraction of high-mass galaxies ($M_\star > 10^{10.5}\mathrm{M}_\odot$) in bins of ρ_2 (right). The dashed vertical line on each plot shows the average matter density. The contour lines on the left panel are at 0.5σ, 1σ, 1.5σ, and 2σ, containing 11.8 per cent, 39.3 per cent, 67.5 per cent, and 86.4 per cent of the points, respectively. The solid lines on the right panel show the mean fraction of high-mass galaxies in density bins across 101 constrained (blue) simulations and 20 unconstrained (red) simulations, with the shaded regions representing the standard deviation across the respective set of simulations. The constrained simulations show a positive correlation between fraction of high-mass galaxies and density, while the unconstrained simulations show no correlation and a very high standard deviation towards high densities.

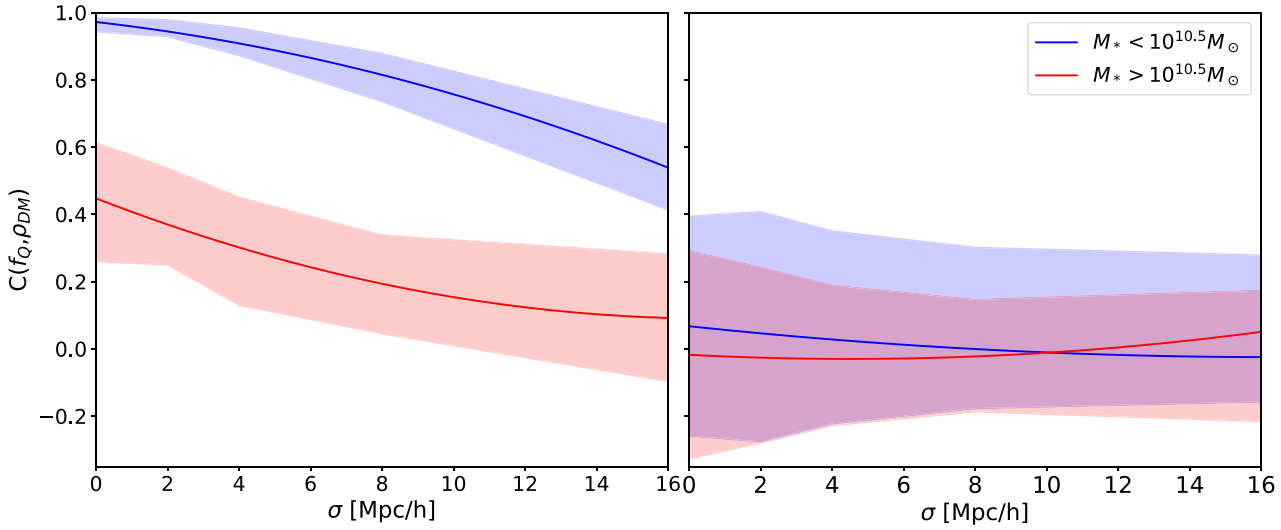

Figure 9. The mean correlation between the fraction of quenched galaxies f_Q and the environmental density ρ_{DM} from constrained simulations (left) and unconstrained simulations (right) as a function of the Gaussian smoothing scale, σ. The solid lines and shading show the mean and 1σ uncertainty across the CSiBORG realizations, respectively. We separately show low-mass (blue, $M_\star < 10^{10.5}\mathrm{M}_\odot$) and high-mass (red, $M_\star > 10^{10.5}\mathrm{M}_\odot$) galaxies. Low-mass galaxies exhibit a much stronger correlation with environment than high-mass galaxies, suggesting that quenching in low-mass galaxies is primarily driven by external mechanisms, while in high-mass galaxies, internal mechanisms play a larger role. See Sections 4.3 and 5.1.2 for further description and analysis of these results.

environment and quenched fraction for low-mass galaxies than high-mass galaxies, in line with Fig. 9. We also see that while quenched fraction continues to increase with ρ_2, it begins to flatten at around 15 Mpc for $\mathrm{d_{fil}}$.

5 DISCUSSION

5.1 Interpretation of results

An advantage of CSiBORG is that the multiple realizations correspond to the uncertainty with which we know the density field. By comparing the correlation strength of each realization of the constrained simulations we can see this uncertainty is subdominant. This implies a low uncertainty due to the BORG posterior. Additionally, bootstrapping galaxies within the sample shows that the uncertainty due to sample size is minimal. The dominant source of uncertainty arises from comparing the correlation from constrained simulations to that from unconstrained simulations, a process described in Section 3.3.

5.1.1 *Star formation and* H I *content*

We now consider the implications of the SFR and $M_{\mathrm{H\,I}}/M_\star$ correlations on models of galaxy formation. Both the NSA and AL-

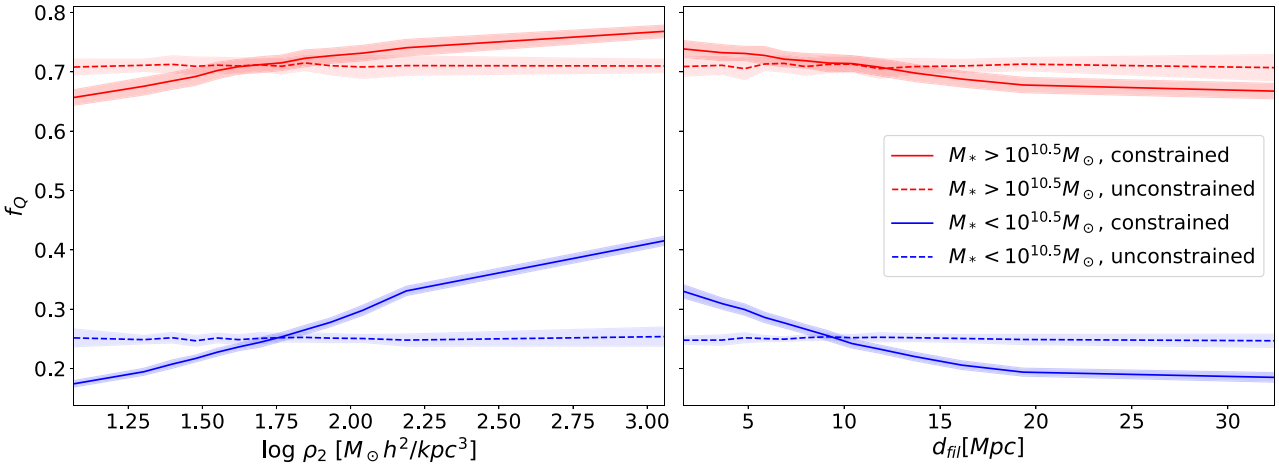

Figure 10. The fraction of quenched galaxies f_Q across bins of ρ_2 (left) and bins of d_{fil} (right) for low-mass (blue, $M_\star < 10^{10.5} M_\odot$) and high-mass (red, $M_\star > 10^{10.5} M_\odot$) galaxies. The solid lines and shading show the mean correlation and its 1σ uncertainty, respectively, for constrained simulations. The dotted lines and shading show the equivalent for unconstrained simulations. f_Q increases as ρ_2 increases, suggesting that greater environmental densities are associated with higher quenching rates. f_Q decreases as d_{fil} increases, indicating that galaxies further from filaments are less likely to experience quenching. f_Q begins to flatten at around $d_{fil} = 15$ Mpc, while f_Q increases for each value of ρ_2. When compared to unconstrained simulations, the plots show that the relationship between f_Q and environment is far stronger for low-mass galaxies than for high-mass galaxies. See Section 5.1.2 for further interpretation of these results.

FALFA correlation results imply that as ρ_{DM} increases, a galaxy is less likely to be star forming, will have a lower $M_{HI}/M_\star$, and will be redder in colour. In the literature, these trends are often attributed to effects such as 'gas heating' (where the intergalactic medium around galaxies is heated by external sources like shocks or AGN feedback, preventing gas from cooling or forming stars, e.g. B. R. McNamara & P. E. J. Nulsen 2007), 'strangulation' (the cessation of cold gas inflow onto a galaxy, e.g. D. Kawata & J. S. Mulchaey 2008), or the effect of 'galaxy group interactions' near filaments (for example ram pressure stripping, mergers, and tidal forces between galaxies which often lead to tidal stripping, e.g. J. E. Gunn & J. R. Gott 1972; E. Roediger & G. Hensler 2005; I. G. McCarthy et al. 2008).

Consistent with the correlations for ρ_{DM}, the results for d_{fil} imply that galaxies closer to filaments have a lower $M_{HI}/M_\star$ and are redder in colour. While of reasonable statistical significance, the direct correlation coefficients are weak. The partial correlations conditioned on $M_\star$ are of negligible statistical significance. Together, these results suggest that gas feeding galaxies from filaments is not strongly prevalent in the local Universe. Our results are qualitatively consistent with K. Kraljic et al. (2018), who find that at lower redshift, filaments are not expected to boost gas flow and therefore increase the quantity of gas or SFR in galaxies. However at high redshifts, the role of the cosmic web is expected to be more important, with gas flow from filaments into galaxies an important effect, as shown by M. Ramsøy et al. (2021).

5.1.2 Quenching

The results presented on the relationship between fraction of quenched galaxies and ρ_{DM} align with P. H. Goubert et al. (2024), who argue that low-mass galaxies experience quenching predominantly due to their environment. P. H. Goubert et al. (2024) link quenching in low-mass galaxies to properties such as host halo mass and galaxy overdensity. On the other hand, they find that quenching in high-mass galaxies is likely to be due to internal processes such as AGN feedback. Our results support this idea, showing that the quenching of high-mass galaxies has a low dependence on environment. This is evident in Fig. 9, where the correlation between ρ_{DM} and quenched fraction is far weaker for high-mass galaxies than low-mass galaxies. N. Porqueres et al. (2018) find that the relationship between AGN properties and environmental density inferred from BORG is more important than the cosmic web structure. However, an alternative possibility is that the most highly quenched galaxies are simply the oldest, residing in the most old and dense haloes, meaning that the observed trend does not necessarily imply AGN-driven quenching. Further confirmation from simulations would be needed to confirm the cause of this quenching.

Fig.9 shows that the correlation between the fraction of quenched galaxies and ρ_{DM} decreases as the degree of smoothing increases. This suggests that the mechanisms driving the quenching of galaxies operate on smaller spatial scales. While the voxel resolution of ρ_0 is 0.7 Mpc h^{-1}, which roughly corresponds to the scale of a cluster-sized halo, the BORG initial conditions are constrained with a voxel resolution four times larger. This could imply that the quenching of low-mass galaxies, with their strong positive correlation at ρ_0, is directly related to the internal processes on the scale of galaxy clusters. This is consistent with the correlations discussed in Section 5.1.1, and evident for the NSA results in Fig. 7: galaxies in higher density environments have lower H I mass content and SFRs, likely due to the processes such as gas heating, strangulation, and the effects of galaxy group environments. We note that the analogous correlations are significantly weaker for the ALFALFA sample, which is dominated by gas-rich, star-forming galaxies and therefore spans a much narrower range in SFR and colour. The strongest correlation between ρ_{DM} and quenched fraction is ρ_0 supporting the idea that the internal processes of a galaxy cluster play a very important role in the quenching of a galaxy.

Fig.10 shows similar trends between the quenched fraction of galaxies in bins of ρ_2 and in bins of d_{fil}. Both show weaker correla-

tions between environment and high-mass galaxies, as expected, and both show steep correlations between low-mass galaxies and environment. The most notable difference between the two, is that the relationship between low-mass galaxies and d_{fil} begins to flatten at around 15 Mpc from the filament. In comparison, the trend with ρ_2 continues to increase with density. This suggests that after a certain distance from filament, the environmental processes linked to quenching are no longer effective. This can be explained by the relationship between d_{fil} and ρ_{DM}, which we show in Fig. 6. There is a steep density gradient close to filaments that begins to flatten at around 15 Mpc from the filament and continues to do so up to 40 Mpc from the filament. W. Wang et al. (2024) find that the maximum density gradient is at 1 Mpc from the filament centre, which suggests that this is where we could expect to see the biggest impact of ram pressure stripping at least. This could suggest that ρ_{DM} is the dominant factor in the environmental quenching of galaxies, as it is the density gradient associated with a filament that is causing quenching, rather than the mechanisms associated with the filamentary structure itself.

5.1.3 Morphology and size

We take the Sérsic index as analogous to the morphology of a galaxy where a Sérsic index of $\lesssim 1.5$ approximately corresponds to disc galaxies, whereas a Sérsic index of $\gtrsim 3$ corresponds to elliptical galaxies. Therefore, our results for NSA correlations suggest that as density increases, the fraction of elliptical galaxies increases. This is in agreement with the theory that elliptical galaxies often form in a 'hierarchical' formation scenario through mergers between galaxies (G. De Lucia et al. 2006). Mergers are more likely in high-density environments due to the increased frequency of close galaxy encounters (see e.g. W. J. Pearson et al. 2024). The correlation of the Sérsic index with d_{fil} supports this idea, suggesting that the closer a galaxy is to a filament, the more likely it is to be elliptical. However, this correlation is weaker than those with ρ_{DM}, suggesting that ρ_{DM} is the dominant factor in influencing the morphology of a galaxy.

The correlation coefficients we find could imply that galaxies of a smaller radius are generally located in higher density areas, particularly when controlling for $M_\star$. However the statistical significance of the correlations for size is low, rendering our results as inconclusive; there is no significant correlation between size and ρ_{DM} or d_{fil}. Nevertheless, this is an interesting result considering conflicting conclusions in the literature. A. Ghosh et al. (2024) investigate the relationship between galaxy size and environment at higher redshifts ($z \geq 0.3$), reporting that *larger* galaxies are more likely to be found in higher density environments, independent of galaxy morphology or stellar mass. This is consistent with F. J. Mercado et al. (2025), who find that low-mass galaxies ($M_\star < 10^9 M_\odot$) are larger if they are experiencing stronger tidal influences (consistent with a higher density environment). This, however, contrasts with our findings at a lower redshift. A. Ghosh et al. (2024) provide a useful analysis of the conflicting galaxy size–environment results throughout the literature. They argue that size is dependent on morphology and $M_\star$, meaning that these factors should be controlled in order to understand the correlation with environment. This could explain the low strength and statistical significance for our correlation between size and environment.

Other studies focusing on the local Universe also show conflicting results. M. Huertas-Company et al. (2013) find that early-type galaxies show no correlation between their mass–size relation and environment, while F. Shankar et al. (2013) find that spheroids in more massive host haloes, where a spheroid is defined as an elliptical galaxy or a galaxy with a large central bulge, have a larger size at fixed $M_\star$. It is worth noting that these studies rely on observations or semi-analytical models, whereas our analysis uses constrained *N*-body simulations, which could account for some differences.

5.1.4 The relative importance of ρ_{DM}, d_{fil}, and σ

Throughout the results and discussion, we compare the correlations found for galaxy properties with ρ_{DM} to those found for galaxy properties with d_{fil}. We find consistently stronger and more statistically significant correlations with ρ_{DM} than with d_{fil}. Additionally, the middle row in Fig. 7, shows that controlling for d_{fil}, gives stronger and more statistically significant correlations than controlling for ρ_{DM}, suggesting that the effects of ρ_{DM} are more significant than the effects of d_{fil}, when considered in isolation. This implies that macroscopic processes occurring due to the structure of the cosmic web itself may not be as relevant in influencing galaxy properties as the processes occurring due to ρ_{DM}. The implications of Fig. 9 are that quenching is driven more by ρ_{DM} than by d_{fil} (explored further in Section 5.1.2). These findings bolster the need for constrained simulations in studies of galactic environment, as ρ_{DM} is otherwise much harder to estimate from the galaxy field than cosmic web structure.

Our analysis compares the effects of different values of σ, representing the degrees of Gaussian smoothing applied to ρ_{DM} (see Section 3.1). Fig. 7 shows that most correlations peak in strength and statistical significance with smoothing scales below 4 Mpc h^{-1}. This provides insight into the scale of interactions that are important in contributing to a galaxy's properties, and is consistent with other studies such as C. C. Lovell et al. (2022) and J. F. Wu, C. K. Jespersen & R. H. Wechsler (2024). We can compare these results to the findings from S. M. Croom et al. (2024), who suggest that a galaxy's properties are primarily dictated by its age and star formation history, with environment playing a secondary role. However, since halo density influences the timing of galaxy formation, the impact of environment is still interconnected with early formation processes, rather than being a purely external factor acting later in a galaxy's evolution.

5.2 Comparison to literature

This section reviews methods for quantifying environment in galaxy studies which focus on *N*-body simulations, hydrodynamical simulations, and observational survey data.

5.2.1 Prior work with constrained N-body simulations

Constrained *N*-body simulations such as ELUCID (H. Wang et al. 2016b) and CSiBORG (D. J. Bartlett et al. 2022; M. L. Hutt et al. 2022; R. Stiskalek et al. 2024), provide a novel framework to study the galaxy and halo relationship with environment. H. Wang et al. (2018) investigate the relationship between galaxy quenching and matter density, finding that quenching correlates with $M_\star$, halo mass, and large-scale matter density, which is consistent with our results. Y. Zhang, X. Yang & H. Guo (2021) find that galaxies with a characteristic subhalo mass below $\sim 10^{12} M_\odot\, h^{-1}$ exhibit a redder colour in nodes, while above the characteristic mass

there is no environmental dependence. Our findings align with these results, as we find a negative correlation between colour and $\rho_{\rm DM}$. We also find that at high $M_\star$, galaxy quenching has a lower correlation with environment than at low $M_\star$, suggesting that internal galaxy processes dominate environmental effects at this scale.

X. Xu et al. (2024) report a correlation of 0.14 between the colour $(g-r)$ of SDSS galaxies, and $\delta_{2.1}$, the matter density contrast for subhaloes in the ELUCID simulation, at a Gaussian smoothing of 2.1 Mpc h^{-1}. Comparatively, we find a correlation of 0.12 between colour $(u-r)$ and ρ_2. Although the measures of environment and colour differ slightly, these correlations show a good degree of consistency. It should however be noted, that the former value does not include an estimation of uncertainty.

An advantage of CSiBORG in comparison to other constrained simulations such as ELUCID, is the availability of 101 realizations, which quantify the reconstruction uncertainty. Additionally, with CSiBORG we compare our results to unconstrained simulations. This allows us to quantify deviations from the null hypothesis that there would be no correlation between a random density distribution and galaxy properties. From this, we produce the significance values in Fig. 7.

5.2.2 Other observational studies

There is substantial literature investigating the correlation between galaxy properties and environment by using observational evidence only (see e.g. K. A. Douglass & M. S. Vogeley 2017; K. Kraljic et al. 2018; M. N. Tudorache et al. 2024; W. Van Kempen et al. 2024; M. Hoosain et al. 2024a). Such studies often quantify environment by using algorithms such as DisPerSE to map the cosmic web structure based on observed (redshift space) galaxy distribution, or by directly estimating the matter density from observational data. For example, both K. Kraljic et al. (2018) and M. Hoosain et al. (2024a) use DisPerSE to map the cosmic web, comparing the distance of a galaxy to cosmic web structures with a galaxy's properties. K. Kraljic et al. (2018) find that more massive and redder galaxies tend to lie closer to filaments and sheets, and that redder galaxies are also preferentially found nearer to nodes. Importantly, they show that even within the star-forming population, galaxies become redder (or have lower sSFRs) as they approach filaments, indicating that some quenching occurs in these environments, independent of stellar mass. They compare their observational findings to the Horizon-AGN simulation (Y. Dubois et al. 2014), finding qualitative agreement. Similarly, M. Hoosain et al. (2024a) find that more massive galaxies tend to lie closer to filaments, and that, independent of stellar mass, galaxies near filaments are redder and more gas deprived. They attribute these trends to the increasing prevalence of galaxy group environments around filaments. Furthermore, for galaxies in low-mass haloes, they find that filaments have an additional effect on their gas content. Fig. 7 highlights the agreement of our results with these findings. In particular we see redder galaxies and lower $M_{\rm H\,I}/M_\star$ content closer to filaments (or in higher density environments). In addition, M. N. Tudorache et al. (2024) analyse the star formation histories from observational data, searching for a link between H I properties and star formation. While they find no significant correlation between peak star formation activity and filament proximity, they note that the two galaxies in their sample located within 1 Mpc of a filament spine are HI deficient and have a very low gas-depletion timescale, suggesting a potential link between a galaxy's properties and its distance to filament.

5.2.3 Comparison to simulations

Correlations between galaxy properties and environment are often studied in hydrodynamical simulations. C. T. Donnan, R. Tojeiro & K. Kraljic (2022) combine observational analyses with IllustrisTNG simulations to find that galaxies closer to nodes have a ∼0.02 dex higher gas-phase metallicity at fixed stellar mass than those further away, to a 5σ significance level with Spearman correlation statistics. In comparison, we find a very low correlation between metallicity and environment, likely because C. T. Donnan et al. (2022) have used a mass–metallicity measurement that is only available for star-forming galaxies, whereas we considered metallicity across the whole NSA data base (with metallicity data that should be 'used with caution', see Section 2.2).

W. Ma, H. Guo & M. G. Jones (2024) use IllustrisTNG together with NeutralUniverseMachine to study how distance to filament affects cold gas content. They find that the role of filaments in affecting H I content is generally much weaker than the effect of halo environment. This is consistent with our result that $\rho_{\rm DM}$ is more significant in affecting galaxy properties than $\rm d_{fil}$.

Hydrodynamical simulations have also been used to investigate the star-forming properties of galaxies (see e.g. C. Byrohl et al. 2024; P. H. Goubert et al. 2024; E. Ko et al. 2024). For example, P. H. Goubert et al. (2024) find lower mass galaxies to be more susceptible to environmental quenching and E. Ko et al. (2024) look at how large-scale structures influence star formation in galaxy clusters. E. Ko et al. (2024) work in the redshift range $0.3 < z < 1.4$, and find that clusters well-connected to surrounding filaments and groups tend to have a lower quenched fraction of galaxies. This contrasts our result that quenched fraction increases in denser environments, and is likely due to the different redshift regimes: at high redshift filaments can feed clusters, while at low- redshift high high-density environments tend to cause quenching.

Hydrodynamical simulations have been useful for studying the scale at which environmental properties are most important. This question is directly analogous to our interest in the most statistically significant degree of Gaussian smoothing. Fig. 1 shows visually how Gaussian smoothing is applied in the CSiBORG simulations. J. F. Wu et al. (2024) use IllustrisTNG to find the connection between galaxies, dark matter haloes and their large-scale environment. They use the DisPerSE algorithm to quantify the distance from cosmic web features, and conclude that overdensity on 2 Mpc h^{-1} scales is the most significant factor (see their Fig. 3). The statistical significance of our results also generally peaks at around 2 Mpc h^{-1}, in good agreement with J. F. Wu et al. (2024). Similarly, C. C. Lovell et al. (2022) report that overdensity on a 2–4 Mpc scale is more important than 1 or 8 Mpc scales, further supporting this conclusion.

A. Storck et al. (2024) probe the linear and non-linear effects of large-scale environment on dark matter halo formation. They find that the mass and virial radius of Milky Way-mass haloes are not significantly affected by environment, with sub- per cent variations. By contrast, the orientation of the halo and its angular momentum relative to the nearest filament is highly sensitive to environment, with changes of 10–80 per cent, and these orientation trends depend on distance to the filament.

Constrained N-body simulations are the way forward in studying galaxy formation and evolution. They offer a comprehensive comparison of the factors affecting the local Universe, whereas no study performed within the scope of a hydrodynamical simulation is guaranteed to represent the observations due to the inherent challenges of galaxy formation modelling. Observational data is essential for validating these models, but constrained simulations overcome the limitations posed by incompleteness and uncertainty quantification that arise when defining the cosmic environment directly from the observed galaxy distribution.

5.3 Future work

There are some known limitations of the CSiBORG suite of simulations introduced in D. J. Bartlett et al. (2022) based on the initial conditions of J. Jasche & G. Lavaux (2019). This version of CSiBORG is known to overpredict cluster masses and the high-mass end of the halo mass function (M. L. Hutt et al. 2022) and only later iterations of CSiBORG have addressed this issue (S. Stopyra et al. 2024). In this work, we assessed the systematic uncertainty of CSiBORG by re-running our analysis using updated, in-development versions of the BORG initial conditions. Following this comparison, we estimate that the systematic uncertainty introduced by CSiBORG is no greater than 3σ. The largest of these uncertainties affects SFR and sSFR, but their correlations remain well above the 5σ significance level. Future applications of CSiBORG to study the galaxy-environment relation would benefit from improved BORG initial conditions and self-consistently deriving the real-space distance using the CSiBORG velocity field.

Research on galaxy formation and evolution could benefit from further categorizing the galaxies and haloes we are studying, expanding on the 'high-mass' and 'low-mass' galaxies we evaluate in this paper. For example, a useful extension would be to categorize galaxies into *satellite galaxies* and *central galaxies* (see e.g. H. Wang et al. 2018; P. H. Goubert et al. 2024). P. H. Goubert et al. (2024), amongst other studies, show that central and satellite galaxies often show clear differences in their physical properties. They report that central galaxies and high-mass satellite galaxies experience quenching due to internal processes while low-mass satellites experience quenching due to environmental effects. H. Wang et al. (2018) also find differences between the quenching of satellite and central galaxies, reporting that satellite galaxies show a strong correlation with environmental density, whereas central galaxies show little to no correlation. When combining these results, they find an overall correlation between environmental density and the fraction of quenched galaxies, which is in agreement with the correlations found in this paper. However, their analysis highlights that there could be nuances within our own data and results which could be explored in future work. It could also be useful to categorize galaxies based on their proximity to other galaxies, differentiating between those galaxies that are members of a group and those that are more isolated (see e.g. W. Van Kempen et al. 2024; M. Hoosain et al. 2024a). This could provide further constraints on the mechanisms responsible for quenching. As discussed in Section 5.1.1, there is extensive literature on the causes of quenching, often with contradicting conclusions. Some state that quenching is due to the location of a galaxy in a group environment, while others argue that it is the lack of access to gas from filament arms or the matter density of a galaxy's environment. Using CSiBORG to investigate separately the effect of environmental density and distance to filament, while differentiating between galaxies that are centrals, satellites, members of a group, or in isolation, would provide useful insight into the significance of each factor.

Further to this, some studies investigate the importance of the mass of the host dark matter haloes in dictating galaxy properties, especially galaxy quenching (H. Wang et al. 2018; W. Ma et al. 2024). Therefore, a useful application of CSiBORG would be to assign halo masses to galaxies and compare the effect of the halo mass on galaxy properties. R. Stiskalek et al. (2024) study the haloes derived from CSiBORG, showing that a halo mass of at least $10^{14}\mathrm{M}_{\odot}$ is required for it to be consistently reconstructed. Thus, the highest mass galaxies can likely by unambiguously matched directly to CSiBORG haloes, whereas a probabilistic matching scheme would be required for lower-mass haloes.

Incorporating those analyses suggested above would require additional modelling and data processing. In particular, identification of centrals and satellites, as well as halo mass assignment, would require either probabilistic matching techniques or additional catalogues not currently used here. A useful first step would be to focus on the most massive haloes and highest-density regions, which can be reconstructed most reliably. We therefore reserve this for future work in order to maintain a clear scope for the present analysis.

It would also be useful to apply our method to hydrodynamical simulations, in order to compare their galaxy–environment correlations to observational results. Since the dark matter density field is easily obtainable in simulations, our method of defining environment provides a better comparison to simulations than those based on observed galaxy catalogues. In addition, applying our method to a hydrodynamical simulation would allow us to investigate the distribution we find in d_{fil}. This is important because generally hydrodynamical simulations don't find d_{fil} for galaxies to be greater than 15 Mpc (e.g. K. Kraljic et al. 2018), whereas many observational studies find much larger separations (e.g. A. Hirv et al. 2017; M. Hoosain et al. 2024b; S. L. Jung et al. 2025). Investigating this difference could help clarify whether our d_{fil} values agree with expectations from simulations, or whether they are affected by factors such as differences in tracer number density.

Lastly, upcoming surveys such as the Large Synoptic Survey Telescope (LSST; Ž. Ivezić et al. 2019), Euclid (R. Laureijs et al. 2011), and the Square Kilometre Array (SKA; R. Maartens et al. 2015) will increase galaxy sample sizes by orders of magnitude and provide unprecedented data quality. Moreover, these data sets will improve sampling of low-mass galaxies, which are underrepresented in current surveys due to their faintness. This will enable a more complete analysis of the relationship between galaxy properties and their environment.

6 CONCLUSION

In this work, we quantify correlations between properties of galaxies and both the local matter density smoothed on various scales and the distance from a cosmic web filament. Galaxy properties are obtained via the NSA and ALFALFA surveys. We define environment using 101 constrained N-body simulations from the CSiBORG suite. We look specifically at correlations with colour, SFR, sSFR, stellar mass, size, Sérsic index, metallicity, and $M_{\mathrm{HI}}/M_{\star}$. Finally, we quantify the relationship between the quenching of high- and low-mass galaxies with their environment, by finding the correlation between quenched fraction of galaxies and their environmental density as well as their distance from a cosmic web filament.

Table 3. Summary of Spearman correlation coefficients with a statistical significance $\geq 5\sigma$.

Spearman Correlation	Survey	Coefficient	Significance
C(colour, $\rho_4 \vert M_\star$)	NSA	0.07	11σ
C(sSFR, ρ_0)	NSA	−0.08	10σ
C(Sérsic index, $\rho_4 \vert M_\star$)	NSA	0.06	9σ
C(colour, ρ_0)	NSA	0.07	8σ
C(colour, $\mathrm{d_{fil}} \vert \mathrm{M}_\star$)	NSA	−0.05	8σ
C(sSFR, $\rho_2 \vert d_{\rm fil}$)	NSA	−0.09	7σ
C(sSFR, $\rho_2 \vert .m._\star$)	NSA	−0.07	7σ
C(Sérsic index, ρ_2)	NSA	0.06	7σ
C(sSFR, $d_{\rm fil}$)	NSA	0.10	6σ
C(sSFR, $d_{\rm fil} \vert \rho_0$)	NSA	0.09	6σ
C(sSFR, $d_{\rm fil} \vert M_\star$)	NSA	0.05	6σ
C(Sérsic index, $\rho_2 \vert d_{\rm fil}$)	NSA	0.05	6σ
C(Sérsic index, $d_{\rm fil} \vert M_\star$)	NSA	−0.04	6σ
C(SFR, ρ_2)	NSA	−0.12	5σ
C(colour, $d_{\rm fil}$)	NSA	−0.09	5σ
C(colour, $d_{\rm fil} \vert \rho_0$)	NSA	−0.08	5σ
C(SFR, $\rho_2 \vert .m._\star$)	NSA	−0.07	5σ
C(Sérsic index, $d_{\rm fil}$)	NSA	−0.05	5σ
C(Size, $\rho_2 \vert .m._\star$)	NSA	−0.05	5σ
C(Size, $d_{\rm fil} \vert M_\star$)	NSA	0.04	5σ
C(Sérsic index, $d_{\rm fil} \vert \rho_0$)	NSA	−0.04	5σ
$C(M_{\rm H\,I}/M_\star, \rho_4)$	ALFALFA	−0.10	8σ
$C(M_{\rm H\,I}/M_\star, d_{\rm fil})$	ALFALFA	0.07	5σ

By using CSiBORG, we are able to measure the underlying dark matter density field, which is a more fundamental probe of environment than metrics based on observed galaxy catalogues. Applying DisPerSE to CSiBORG allows us to map out the cosmic web structure of the Universe, defining the positions of nodes, sheets, filaments and voids. We thus quantify the galaxy–environment connection, defining environment in two ways: environmental density ($\rho_{\rm DM}$), and distance from filament ($\mathrm{d_{fil}}$). The correlations with the highest statistical significance are summarized in Table 3. The key conclusions of the paper are as follows:

(i) CSiBORG provides a robust and reliable way to quantify environment, as it provides a complete and accurate representation of the dark matter distribution in the local Universe. A major advantage of using CSiBORG is that its multiple realizations characterize the uncertainty with which the field is reconstructed. Additionally, a comparison to unconstrained simulations can be used to find the statistical significance of the results.

(ii) Defining the cosmic environment as the dark matter density environment of a galaxy, rather than its location in the cosmic web, produces stronger correlations and greater statistical significance. This suggests that environmental density has a greater impact on galaxy properties than the position of a galaxy in the cosmic web, as is perhaps not surprising given that the cosmic web simply summarizes the density field. It also further highlights the importance of the constrained simulations: while a proxy to the cosmic web can be obtained from the observed distribution of galaxies, it is much more difficult to obtain the dark matter field due to the complex phenomenon of galaxy bias.

(iii) We find statistically significant negative correlations between the environmental density and SFR, sSFR and H I-mass–stellar-mass ratio as well as positive correlations with colour and environmental density. Together, these correlations suggest that bluer, more HI rich galaxies tend to be found in less dense areas. This is likely due to environmental processes which occur in high-density environments, such as gas heating, strangulation, and the effects of galaxy group environments.

(iv) The quenching of low-mass galaxies ($M_\star < 10^{10.5}\mathrm{M}_\odot$) has a greater dependence on environmental density than the quenching of high-mass galaxies ($M_\star > 10^{10.5}\mathrm{M}_\odot$). This is because low-mass galaxies generally undergo quenching due to environmental factors, while high-mass galaxies are more often quenched due to internal processes such as AGN feedback.

In summary, we find statistically significant correlations between properties of galaxies and their corresponding cosmic web environment. This has enabled us to gain insight into the processes which govern galaxy formation and evolution. The correlations calculated in this paper can be used to test theoretical models of galaxy formation, and enable us to place further constraints on the significance of astrophysical processes on galaxy formation. We demonstrate the ability of constrained simulations to pinpoint the relationships between galaxies and their environments, underlining their importance as a method with which to define the dark matter environments of the local Universe.

ACKNOWLEDGEMENTS

We thank Jens Jasche, Madalina Tudorache and Adriano Poci for useful inputs and discussion.

CG, TY and MJ acknowledge support from a UKRI Frontiers Research Grant [EP/X026639/1], which was selected by the ERC. CG also acknowledges support from the Oxford University Astrophysics Summer Research programme. RS acknowledges financial support from STFC Grant No. ST/X508664/1, the Snell Exhibition of Balliol College, Oxford, and the CCA Pre-doctoral Program. HD is supported by a Royal Society University Research Fellowship (grant no. 211046).

This project has received funding from the European Research Council (ERC) under the European Union's Horizon 2020 research and innovation programme (grant agreement no. 693024). We also thank Jonathan Patterson for smoothly running the Glamdring Cluster hosted by the University of Oxford, where the data processing was performed.

DATA AVAILABILITY

Data from the NSA, ALFALFA, and MPA-JHU surveys is publicly available at http://nsatlas.org, https://egg.astro.cornell.edu/alfalfa/data/, and https://wwwmpa.mpa-garching.mpg.de/SDSS/DR7/. Other data underlying the article will be made available upon reasonable request.

REFERENCES

Abazajian K. N. et al., 2009, ApJS, 182, 543
Aihara H. et al., 2011, ApJS, 193, 29
Angulo R. E., Hahn O., 2022, Living Reviews in Computational Astrophysics, 8, 1
Bahcall N. A., 1999, in Dekel A., Ostriker J. P., eds, Formation of Structure in the Universe. Cambridge University Press, Cambridge, p. 137
Barsanti S. et al., 2023, MNRAS, 526, 1613
Bartlett D. J., Desmond H., Ferreira P. G., 2021, Phys. Rev. D, 103, 023523
Bartlett D. J., Kostić A., Desmond H., Jasche J., Lavaux G., 2022, Phys. Rev. D, 106, 103526
Behroozi P., Wechsler R. H., Hearin A. P., Conroy C., 2019, MNRAS, 488, 3143

Bluck A. F. L., Mendel J. T., Ellison S. L., Moreno J., Simard L., Patton D. R., Starkenburg E., 2014, MNRAS, 441, 599
Boldrini P., Laigle C., 2025, A&A, 700, A182
Bower R. G., Benson A. J., Malbon R., Helly J. C., Frenk C. S., Baugh C. M., Cole S., Lacey C. G., 2006, MNRAS, 370, 645
Bower R. G., Schaye J., Frenk C. S., Theuns T., Schaller M., Crain R. A., McAlpine S., 2017, MNRAS, 465, 32
Brinchmann J., Charlot S., White S. D. M., Tremonti C., Kauffmann G., Heckman T., Brinkmann J., 2004, MNRAS, 351, 1151
Byrohl C., Nelson D., Horowitz B., Lee K.-G., Pillepich A., 2025, A&A, 698, A103
Cappellari M., 2016, ARA&A, 54, 597
Cleveland W. S., 1979, Journal of the American Statistical Association, 74, 829
Colombi S., Chodorowski M. J., Teyssier R., 2007, MNRAS, 375, 348
Cortese L., Catinella B., Boissier S., Boselli A., Heinis S., 2011, MNRAS, 415, 1797
Croom S. M. et al., 2024, MNRAS, 529, 3446
Croton D. J. et al., 2006, MNRAS, 365, 11
Cui W., Davé R., Peacock J. A., Anglés-Alcázar D., Yang X., 2021, Nat. Astron., 5, 1069
Davis M., Efstathiou G., Frenk C. S., White S. D. M., 1985, ApJ, 292, 371
De Lucia G., Springel V., White S. D. M., Croton D., Kauffmann G., 2006, MNRAS, 366, 499
Desmond H., Hutt M. L., Devriendt J., Slyz A., 2022, MNRAS, 511, L45
Doeser L., Jamieson D., Stopyra S., Lavaux G., Leclercq F., Jasche J., 2024, MNRAS, 535, 1258
Donnan C. T., Tojeiro R., Kraljic K., 2022, Nat. Astron., 6, 599
Douglass K. A., Vogeley M. S., 2017, ApJ, 834, 186
Dressler A., 1980, ApJ, 236, 351
Dubois Y. et al., 2014, MNRAS, 444, 1453
Dubois Y., Peirani S., Pichon C., Devriendt J., Gavazzi R., Welker C., Volonteri M., 2016, MNRAS, 463, 3948
Galárraga-Espinosa D. et al., 2024, A&A, 684, A63
Ghosh A., Urry C. M., Powell M. C., Shimakawa R., van den Bosch F. C., Nagai D., Mitra K., Connolly A. J., 2024, ApJ, 971, 142
Gottloeber S., Hoffman Y., Yepes G., 2010, preprint (arXiv:1005.2687)
Goubert P. H., Bluck A. F. L., Piotrowska J. M., Maiolino R., 2024, MNRAS, 528, 4891
Gunn J. E., Gott III J. R., 1972, ApJ, 176, 1
Haynes M. P. et al., 2018, ApJ, 861, 49
Hess K. M., Wilcots E. M., 2013, AJ, 146, 124
Hirv A., Pelt J., Saar E., Tago E., Tamm A., Tempel E., Einasto M., 2017, A&A, 599, A31
Hoosain M. et al., 2024a, MNRAS, 528, 4139
Hoosain M. et al., 2024b, MNRAS, 528, 4139
Huertas-Company M., Shankar F., Mei S., Bernardi M., Aguerri J. A. L., Meert A., Vikram V., 2013, ApJ, 779, 29
Hutt M. L., Desmond H., Devriendt J., Slyz A., 2022, MNRAS, 516, 3592
Ivezić Ž. et al., 2019, ApJ, 873, 111
Jasche J., Lavaux G., 2019, A&A, 625, A64
Jasche J., Wandelt B. D., 2013, MNRAS, 432, 894
Jasche J., Leclercq F., Wandelt B. D., 2015, J. Cosmol. Astropart. Phys., 2015, 036
Jung S. L., Whittam I. H., Jarvis M. J., Hale C. L., Tudorache M. N., Yasin T., 2025, MNRAS, 539, 2362
Kauffmann G. et al., 2003, MNRAS, 341, 33
Kawata D., Mulchaey J. S., 2008, ApJ, 672, L103
Kendall M. G., Stuart A., 1973, The Advanced Theory of Statistics, Volume 2: Inference and Relationship. Charles Griffin & Co. Ltd., London, Section: 31.18
Ko E., Im M., Lee S.-K., Laigle C., 2024, ApJ, 976, 154
Kostić A., Bartlett D. J., Desmond H., 2023, preprint (arXiv:2304.10301)
Kraljic K. et al., 2018, MNRAS, 474, 547
Kraljic K., Duckworth C., Tojeiro R., Alam S., Bizyaev D., Weijmans A.-M., Boardman N. F., Lane R. R., 2021, MNRAS, 504, 4626
Laureijs R. et al., 2011, preprint (arXiv:1110.3193)
Lavaux G., Hudson M. J., 2011, MNRAS, 416, 2840
Lavaux G., Jasche J., 2016, MNRAS, 455, 3169
Leclercq F., 2015, PhD thesis, Institut d'Astrophysique de Paris
Libeskind N. I. et al., 2018, MNRAS, 473, 1195
Lovell C. C., Wilkins S. M., Thomas P. A., Schaller M., Baugh C. M., Fabbian G., Bahé Y., 2022, MNRAS, 509, 5046
Ma W., Guo H., Jones M. G., 2025, A&A, 695, A5
Maartens R., Abdalla F. B., Jarvis M., Santos M. G., 2015, preprint (arXiv:1501.04076)
Macciò A. V., Dutton A. A., van den Bosch F. C., Moore B., Potter D., Stadel J., 2007, MNRAS, 378, 55
Martin D. C. et al., 2005, ApJ, 619, L1
Matthee J., Schaye J., Crain R. A., Schaller M., Bower R., Theuns T., 2017, MNRAS, 465, 2381
McCarthy I. G., Frenk C. S., Font A. S., Lacey C. G., Bower R. G., Mitchell N. L., Balogh M. L., Theuns T., 2008, MNRAS, 383, 593
McLure R. J. et al., 2013, MNRAS, 428, 1088
McNamara B. R., Nulsen P. E. J., 2007, ARA&A, 45, 117
Mercado F. J. et al., 2025, ApJ, 983, 93
Milner J. W., 1963, Discrete Morse Theory. Princeton Univ. Press, New York
Monaghan J. J., 1992, ARA&A, 30, 543
Naab T., Johansson P. H., Ostriker J. P., 2009, ApJ, 699, L178
Novosyadlyj B., Tsizh M., 2017, Condensed Matter Physics, 20, 13901
Odekon M. C. et al., 2016, ApJ, 824, 110
Palla F., Salpeter E. E., Stahler S. W., 1983, ApJ, 271, 632
Pearson W. J. et al., 2024, A&A, 686, A94
Peng Y.-J. et al., 2010, ApJ, 721, 193
Perez I. et al., 2025, A&A, 695, A84
Porqueres N., Jasche J., Enßlin T. A., Lavaux G., 2018, A&A, 612, A31
Ramsøy M., Slyz A., Devriendt J., Laigle C., Dubois Y., 2021, MNRAS, 502, 351
Roediger E., Hensler G., 2005, A&A, 433, 875
Schaap W. E., van de Weygaert R., 2000, A&A, 363, L29
Schaye J. et al., 2015, MNRAS, 446, 521
Shankar F., Marulli F., Bernardi M., Mei S., Meert A., Vikram V., 2013, MNRAS, 428, 109
Solanes J. M., Manrique A., García-Gómez C., González-Casado G., Giovanelli R., Haynes M. P., 2001, ApJ, 548, 97
Sorce J. G. et al., 2016, MNRAS, 455, 2078
Sousbie T., Pichon C., Kawahara H., 2011a, MNRAS, 414, 384
Sousbie T., Pichon C., Kawahara H., 2011b, MNRAS, 414, 384
Stiskalek R., Desmond H., Holvey T., Jones M. G., 2021, MNRAS, 506, 3205
Stiskalek R., Desmond H., Devriendt J., Slyz A., 2024, MNRAS, 534, 3120
Stiskalek R., Desmond H., Devriendt J., Slyz A., Lavaux G., Hudson M. J., Bartlett D. J., Courtois H. M., 2025, MNRAS, 545, staf1960
Stopyra S., Peiris H. V., Pontzen A., Jasche J., Lavaux G., 2024, MNRAS, 527, 1244
Storck A., Cadiou C., Agertz O., Galárraga-Espinosa D., 2024, MNRAS, 539, 487
Tempel E., Libeskind N. I., 2013, ApJ, 775, L42
Tempel E., Stoica R. S., Martínez V. J., Liivamägi L. J., Castellan G., Saar E., 2014, MNRAS, 438, 3465
Tremonti C. A. et al., 2004, ApJ, 613, 898
Tudorache M. N. et al., 2022, MNRAS, 513, 2168
Tudorache M. N. et al., 2024, preprint (arXiv:2411.14940)
Van Kempen W. et al., 2024, PASA, 41, e096
Wang H. et al., 2016a, ApJ, 831, 164
Wang H. et al., 2016b, ApJ, 831, 164
Wang H. et al., 2018, ApJ, 852, 31
Wang W. et al., 2024, MNRAS, 532, 4604
Wang Y., Zehavi I., Contreras S., Cole S., Norberg P., 2025, ApJ, 988, 280
Wechsler R. H., Bullock J. S., Primack J. R., Kravtsov A. V., Dekel A., 2002, ApJ, 568, 52
Whitaker K. E., van Dokkum P. G., Brammer G., Franx M., 2012, ApJ, 754, L29
Willick J. A., Courteau S., Faber S. M., Burstein D., Dekel A., Strauss M. A., 1997, ApJS, 109, 333

Wu J. F., Jespersen C. K., Wechsler R. H., 2024, ApJ, 976, 37
Xu X., Yang X., Xu H., Zhang Y., 2024, MNRAS, 527, 7013
Yang X. et al., 2018, ApJ, 860, 30
York D. G. et al., 2000, AJ, 120, 1579
Zehavi I., Contreras S., Padilla N., Smith N. J., Baugh C. M., Norberg P., 2018, ApJ, 853, 84
Zel'dovich Y. B., 1970, A&A, 5, 84
Zhang Y., Yang X., Wang H., Wang L., Luo W., Mo H. J., van den Bosch F. C., 2015, ApJ, 798, 17
Zhang Y., Yang X., Guo H., 2021, MNRAS, 507, 5320
Zhang Y., Yang X., Guo H., 2022, MNRAS, 517, 3579
Zheng Y., Xu K., Zhao D., Jing Y. P., Gao H., Luo X., Li M., 2025, ApJ, 984, 193

This paper has been typeset from a TEX/LATEX file prepared by the author.